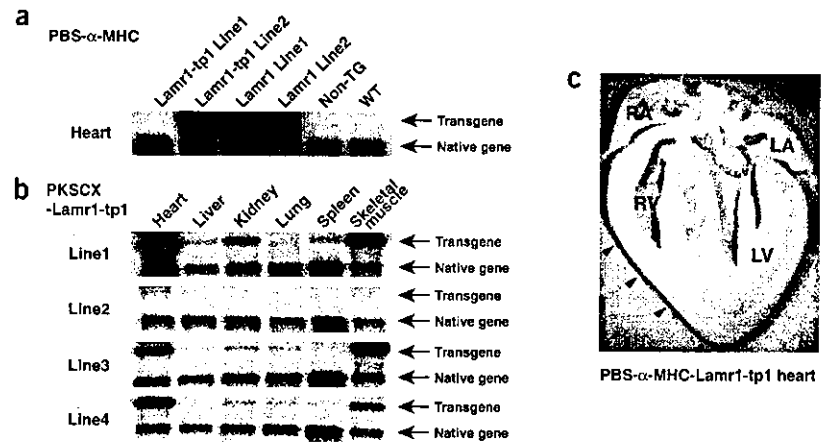

Figure 5 Expressional (northern blot) analysis both of the transgenes and native genes in each transgenic mouse model. *Lamr1-tp1* and *Lamr1* were detected in equal amounts in this analysis. (**a**) Transgene expression in heart samples from two strains of PBS-α-MHC-Lamr1-tp1 mice, two strains of PBS-α-MHC-Lamr1 mice and a control (WT) mouse strain. Non-TG, nontransgenic strain. (**b**) Comparison of gene expression by four lines of the transgenic mouse model PKSCX-Lamr1-tp1 in which transgenes were systemically expressed. (**c**) The complete change to the right ventricle is shown in a macroscopic view of a PBS-α-MHC-Lamr1-tp1 heart from a 10-week-old mouse. LA, left atrium; LV, left ventricle; RA, right atrium; RV, right ventricle.

showed only slight damage at the injection site and the GPF$^+$ cells were healthy, showing no degradation (**Fig. 4d–f**). Fibrous tissue was rarely seen in the hearts transfected with *Lamr1*.

We analyzed further the role of LAMR1-TP1 using transgenic mice. We generated two strains of transgenic mice that expressed *Lamr1* either systemically (with a KSCX promoter) or only in the heart (with an α-MHC promoter). We then established six substrains of *Lamr1-tp1* transgenic mice (four with KSCX promoters and two with α-MHC promoters) and four substrains of *Lamr1* transgenic mice (**Fig. 5a,b**). Among the six strains of *Lamr1-tp1* transgenic mice, four strains showed cardiac expression of the LAMR1-TP1 product.

All four strains expressed LAMR1-TP1 in the heart and were extremely susceptible to RVD (**Fig. 5c**). Sometimes the tissue damage extended to the left ventricle, but right ventricle involvement was always predominant. So far, no phenotypic changes have been detected in the other organs of *Lamr1-tp1* transgenic mice. In contrast, all strains that expressed LAMR1 showed no marked changes in any organ, including the heart. These data indicated that LAMR1-TP1 was responsible for RVD in KK/Rvd mice.

In vitro role of LAMR1-TP1

The *in vitro* expression of LAMR1-TP1 also impaired cardiomyocyte function. Cultured rat cardiomyocytes were transfected with an adenovirus vector containing Lamr1-tp1-IRES-GFP and Lamr1-IRES-GFP under the control of a CA promoter. To clarify the effects of these constructs, we carried out an MTS assay. Only expression of *Lamr1-tp1* by cardiomyocytes led to a decrease of cell numbers 48 h after transfection (**Fig. 6a**), even though the same transfection efficiency was confirmed in all groups based on the level of GFP expression (**Fig. 6b**). On histochemical staining, the most prominent change in these cells was alteration of the chromatin architecture. Staining of heterochromatin by DAPI showed a mosaic pattern in cardiomyocytes transfected with *Lamr1* and a speckled pattern in cardiomyocytes transfected with *Lamr1-tp1*.

We analyzed the localization of LAMR1 and LAMR1-TP1 by confocal microscopy. Rat cardiomyocytes transfected with an adenovirus vector were stained using a LAMR1 antibody (FD4818). This antibody could not distinguish LAMR1 from LAMR1-TP1, but only transfected proteins were stained because endogenous LAMR1 was not detected at its relatively low level of expression. LAMR1 was identified in the DAPI-negative euchromatin area of the nucleus, showing a mirror image to the pattern of DAPI staining (**Fig. 6c**). On the other hand, transfection with *Lamr1-tp1* altered the overall pattern of chromatin as described above and LAMR1-TP1 was partially colocalized with the DAPI-positive heterochromatic loci (**Fig. 6c**). These structural changes to chromatin were observed 10–12 h after transfection and preceded the onset of decreasing cell numbers 24 h after transfection.

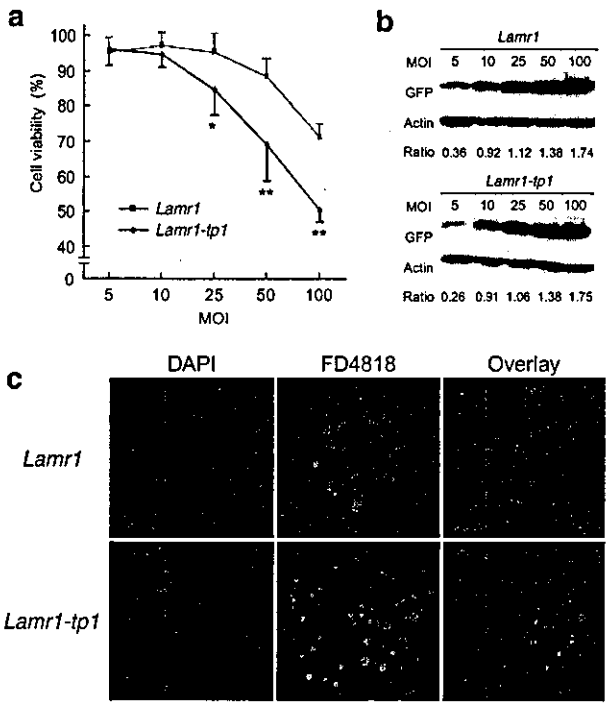

Figure 6 *Lamr1-tp1* caused cardiomyocyte cell death. Cardiomyocytes were infected with recombinant adenoviruses at the indicated multiplicity of infection (MOI). (**a**) Cells expressing *Lamr1-tp1* show lower MTS activity 48 h after adenovirus infection. $^*P < 0.05$ versus *Lamr1*; $^{**}P < 0.005$ versus *Lamr1*. (**b**) GFP and actin expression were analyzed 8 h after adenovirus infection. Cell numbers were equivalent at this time point. The ratios of densitometric measurement of GFP:actin are indicated. (**c**) The nuclei of rat cardiomyocytes expressing Lamr1-IRES-GFP or Lamr1-tp1-IRES-GFP were stained with the LAMR1 antibody FD4818 (green) and DAPI (blue). LAMR1 staining showed a perfect mirror image to DAPI-positive area. LAMR1-TP1 was translocated and partially overlapped with DAPI-positive. Scale bar, 20 μm.

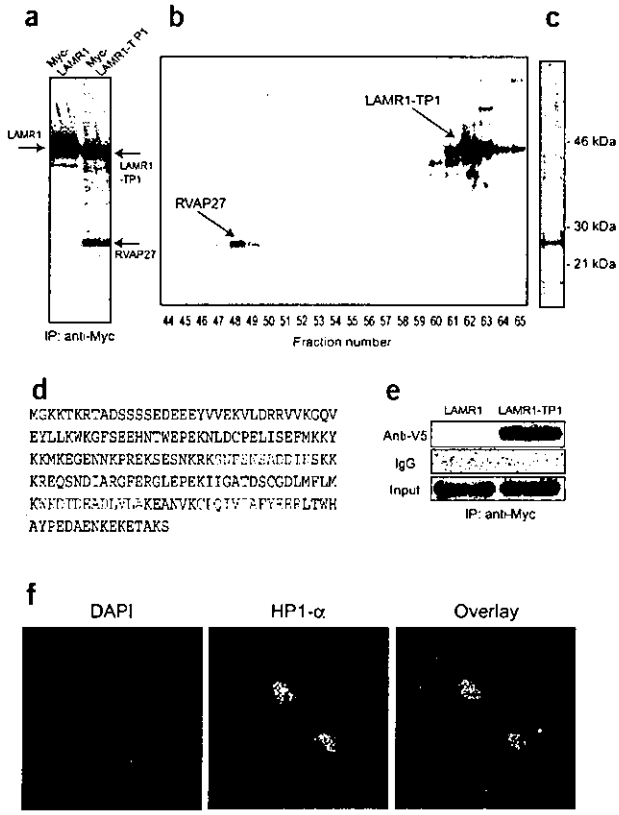

Figure 7 LAMR1-TP1 interacts with HP1-α. (**a**) RVAP27 was immunoprecipitated with LAMR1-TP1 but not with LAMR1 in COS7 cells labeled by ^{35}S-cystein and methionine. (**b**) The complex of radiolabeled LAMR1-TP1 and RVAP27 was separated by a phenyl reverse-phase column. (**c**) The final purification product of RVAP27 was silver-stained. (**d**) The peptides derived from the purified protein, which fitted with those of human HP1-α (as assessed by direct N-terminal sequencing (red) or liquid chromatography-mass spectrometry or mass spectrometry (blue)), are underlined. Cytokine was detected as a Cys-S-propionamide. (**e**) V_5-LAMR1-TP1 but not V_5-LAMR1 expressed in COS7 cells was immunoprecipitated with Myc-tagged HP1-α by anti-Myc. IgG was derived from nonimmunized serum. (**f**) Rat cardiomyocytes were stained with HP1-α antibody, showing HP1-α localization with the DAPI-positive heterochromatin area.

The data suggested that these chromatin changes might have had a lethal effect on the cardiomyocytes, although the possibility that these changes were secondary to lethal cell damage itself cannot be fully excluded.

HP1 binds to mutant LAMR1

To clarify the cellular mechanism by which LAMR1-TP1 caused conformational changes of heterochromatin, we purified and cloned the protein specifically interacting with LAMR1-TP1. The Myc-tagged LAMR1-TP1 fusion protein expressed in ^{35}S-labeled COS7 cells showed the same migration pattern as Myc-tagged LAMR1 (**Fig. 7a**). This 27-kDa protein (named RVAP27) was immunoprecipitated with LAMR1-TP1 but not with LAMR1. Using either a mouse cell line (3T3) or rat cardiomyocytes, we also immunoprecipitated RVAP27 with transfected LAMR1-TP1. Large-scale purification of RVAP27 was done by the sequential use of columns (**Fig. 7b**), and about 10 pmol of RVAP27 was purified from the lysate of 1.0×10^8 COS7 cells (**Fig. 7c**). We analyzed the peptides digested from the RVAP27 band by Edman degradation N-terminal sequencing or nanoelectrospray ionization tandem mass spectrometry. RVAP27 included fragments of the amino acid sequences of SNFSNSADDIK, WKDTDEADLVLA and CPQIVI-AFYEER that matched human heterochromatin protein 1-α (HP1-α) (**Fig. 7d**). The Myc antibody coprecipitated Myc-tagged HP1-α with V_5-tagged LAMR1-TP1, but not with LAMR1; this verified the specific interaction between HP1-α and LAMR1-TP1 (**Fig. 7e**).

HP1 is a key heterochromatin protein that regulates gene silencing by interacting with methylated histones[17]. HP1-α also localizes with DAPI-positive heterochromatin[18]. Cardiomyocytes expressing HP1-α showed the same staining pattern in the DAPI-dense region (**Fig. 7f**). Our immunohistochemical data showed that LAMR1 localized to the euchromatin (DAPI-negative) and that LAMR1-TP1 was partially translocated to heterochromatin (DAPI-positive; **Fig. 6c**). These findings imply that the mutant LAMR1 had an increased affinity for HP1-α and thus was translocated to heterochromatin. Such translocation might influence transcriptional regulation and interfere with the expression of genes essential to the survival of cardiomyocytes, leading to lethal cell dysfunction due to LAMR1-TP1.

Changes of gene expression induced by LAMR1-TP1

To investigate transcriptional regulation by LAMR1-TP1, we analyzed changes in gene expression in cultured cardiomyocytes after transfection of *Lamr1-tp1* or *Lamr1*. Because cells expressing *Lamr1-tp1* began to die 24 h after transfection, we analyzed gene expression at 6 h, 12 h and 24 h (each in duplicate) to exclude the secondary effects of lethal cell damage. GFP expression indicated that the transfected protein was expressed 10 h after transfection, indicating that the expression of genes at 6 h was largely induced by viral infection itself. Transfection with wild-type LAMR1 had a minimal effect on the expression profile compared with that of nontransfected cardiomyocytes, even though the adenovirus vector itself should cause some cell damage (**Supplementary Fig. 1** online). On the other hand, LAMR1-TP1 caused substantial changes in gene expression at 12 h and 24 h, but not at 6 h (**Supplementary Table 1** online). These genes showed similar changes in expression in duplicate analyses. We confirmed further the expression of these genes by quantitative PCR (**Supplementary Fig. 1** online). Our results suggested that LAMR1-TP1, but not LAMR1, could alter the expression of some specific genes. How these genes actually determine the fate of cardiomyocytes needs to be determined in order to understand the pathological role of this mutant protein.

DISCUSSION

Although lethal tachyarrhythmia is often detected in human ARVD, we did not detect it in this mouse model. The difficulty in generating lethal tachyarrhythmia in mice, due to the high beating rate and small size of their hearts[19], might explain our failure to detect lethal arrhythmia. KK/Rvd mice showed electric conduction inhomogeneity leading to prolonged QRS duration, which is often seen in humans with ARVD[20,21]. If similar degradation occurs in the human heart, it will become a focus for lethal arrhythmia at some stage in life. The most important pathological feature of ARVD is the degeneration of right ventricular cardiomyocytes[22]. Our ARVD mouse model reproduced the specific right ventricular degeneration from the outside inwards.

It is still not known why the right ventricle is more susceptible than the left ventricle in these mice. Injection of *Lamr1-tp1* into the left ventricle also induced cardiomyocyte degeneration and calcification,

Table 1 Comparison of human *LAMR1* and histone-related gene loci with ARVD loci

ARVD candidate locus	*LAMR1* related gene	Histone-related gene
ARVD4, 2q32.1–32.3	XM_013127*, 2q31	*HAT1*, 2q31.2–33.1
ARVD5, 3p23	*LAMR1*, 3p21	
ARVD6, 10p12–14	XM_053952*, 10p14	

HAT1, histone acetyl transferase 1; asterisks, *LAMR1* retroposons.

but the changes were less severe (data not shown). Also, transgenic mice that expressed LAMR1-TP1 in both cardiac chambers showed predominant right ventricular degeneration. It seems possible that the threshold for cardiomyocyte damage is higher in the left ventricle than in the right ventricle. This implies that a higher level of *Lamr1-tp1* expression could cause left ventricular degeneration. Often in human ARVD, a part of the left ventricle is involved. Although both ARVD2 and Naxos disease show a right ventricle–specific phenotype in humans, the genes responsible are equally expressed in both cardiac chambers[6,23]; the mechanism of right ventricular susceptibility is still unknown. The most likely explanation is that specific genes that determine the susceptibility to cell damage exist in either ventricle. Left ventricular cardiomyocytes are under high stress because of the high pressure in this ventricle, and more cytoprotective genes may be induced as a result. In fact, microarray analysis comparing right ventricle and left ventricle shows higher expression in the left ventricle of genes belonging to the category of cell and organism defense[24]. Dominant degeneration of the outer right ventricular wall in ARVD also supports this concept because the inner free wall is under more mechanical stress and expresses more defensive genes, such as heat shock proteins. This mechanism might lead to left ventricle protection in ARVD. Alternatively, right ventricle–specific genes may be involved in the susceptibility of the right ventricle. Mice lacking the right ventricle–specific gene actinin-associated LIM-domain protein show some ARVD-like features[25], even though the histological characteristics are considerably different from those of human ARVD.

We found that one of the heterochromatin complex proteins, HP1-α, showed specific binding to LAMR1-TP1. HP1-α is a key component of condensed DNA and is involved in gene silencing by interaction with methylated histone H3. Mobility of HP1-α has been reported in various cells[18,26]. The stochastic competition between such factors as LAMR1-TP1 and HP1-α may determine the fate of the heterochromatin plasticity that is involved in regulating the fate of cells. Class II histone deacetylase acts as a signal-responsive suppressor of the transcriptional events governing cardiac hypertrophy and heart failure[27]. HP1 can link with class II histone deacetylase[28] and thus may modify cardiac cell metabolism. Accordingly, we conclude that LAMR1-TP1 was translated from an active retroposon in ARVD mice and then interacted with HP1-α, leading to the early death of cardiomyocytes.

Genomic databases indicate that there are up to 40 and 32 *Lamr1* retroposons in humans and mice, respectively. It has also been suggested that the *Lamr1* gene family in mammals, with the exception of the functional locus, is comprised entirely of retrotransposons or processed pseudogenes. Most processed retroposons are not expressed and have no functional activity, but several active retroposons or pseudogenes have been identified[29–32]. We show that the active retroposon may cause the pathological condition of ARVD. In humans, a highly conserved mutated form of *Lamr1* has been isolated from a fetal brain cDNA library[33], suggesting that mutant LAMR1 proteins are also transcribed in humans. Several reported human ARVD loci are located close to the retroposons of *Lamr1* or histone-modulating protein genes (Table 1), suggesting that either LAMR1 or HP1 may cause hereditary RVD in humans.

METHODS

PWK mouse strain. The PWK strain belongs to the *Mus musculus musculus* subspecies, which separated from *Mus musculus domesticus* some 1 million years ago. It is maintained as one of the wild-type–derived inbred strains.

***Lamr1-tp1* expressional analysis.** We carried out PCR assays to confirm the presence of each identified mutation. Mismatch assays for the 287T→C and 291G→T mutations in the nucleic acid sequence of *Lamr1* introduced changes at the penultimate 3′ position for the forward primer and 868C→T for the reverse primer, respectively (primer sequences available on request). Each PCR product was digested with *Nhe*I (specific for *Lamr1-tp1* amplicon) to produce fragments of 334 bp and 279 bp; the *Lamr1* amplicon was uncut.

Injection of recombinant DNA *in vivo*. Female C57Bl/6 mice (8 weeks old, 22–25 g) were anesthetized with a mixture of ketamine (100 mg per kg body weight intraperitoneally) and xylazine (5 mg kg body weight intraperitoneally), intubated and ventilated. We carried out a left lateral thoracotomy to expose the beating heart and injected 10 μg of plasmid DNA in 100 μl of phosphate-buffered saline containing 5% sucrose into the right ventricular wall with a 30-gauge needle. The mice were killed 3 weeks after injection and histological staining was done.

Transgenic mice models. We constructed three kinds of targeting vectors under the following promoters (*Lamr1-tp1*, KSCX and α-MHC; *Lamr1*, α-MHC). We introduced these targeting vectors into blastocysts (derived from the C57Bl/6 Jcl mouse strain) by a standard pronuclear microinjection technique[34].

Preparation of adenovirus. Replication-defective recombinant adenoviral vectors expressing Lamr1-tp1-IRES-GFP and Lamr1-IRES-GFP were prepared with the adenovirus expression vector kit following the manufacturer's protocol (Takara). Briefly, *Lamr1-tp1* and *Lamr1* cDNA connected to an IRES-GFP sequence (Clontech) were placed after a CA promoter that was composed of a cytomegalovirus enhancer; a chicken β-actin promoter and rabbit β-globin poly(A) were inserted into a cassette cosmid vector that contained an entire adenovirus type 5 genome except for the E1a, E1b and E3 regions. A recombinant adenovirus was constructed by *in vitro* homologous recombination in HEK293 cells with the use of this cosmid vector and the adenovirus DNA terminal-protein complex. The desired recombinant adenovirus was purified by ultracentrifugation through a $CsCl_2$ gradient followed by extensive dialysis. The titer of the virus stock was assessed by a plaque formation assay that used the HEK293 cells. Cardiomyocytes were infected with the recombinant adenovirus vectors at a multiplicity of infection of 5–100 plaque-forming units per cell. We assessed the expression of GFP and β-actin by immunoblotting with 20 μg of myocardial protein lysate.

Primary culture of neonatal rat ventricular myocytes and MTS assay. Ventricular myocytes obtained from 1- or 2-d-old Wister rats were prepared and cultured overnight in Dulbecco's modified Eagle medium containing 10% fetal bovine serum as described[35]. Cytotoxicity was assessed with a CellTiter 96 Aqueous One Solution Cell Proliferation Assay System (Promega). Rat cardiomyocytes were cultured in 96-well culture plates at a density of 3×10^4 cells cm^{-2}. MTS reagent was added to each well 48 h after the addition of adenovirus to the myocytes. After a 1-h incubation period, optical absorbance at 490 nm was measured with a microplate reader. Cell viability was expressed as mean percentages for the absorbance at multiplicity of infection of 5 with the standard deviations of absorbance.

Antibodies. We used antibodies to MCP-1 (Santa Cruz Biotechnology), GFP, Myc-conjugate beads (Clontech), V_5 (Invitrogen) and HP1-α (Upstate Biotechnology). The polyclonal antibody FD4818 was derived from rabbits against the amino acid sequence RALNVLQMKEEDVFK, which corresponds to amino acids 3–15 of LAMR1.

Identification of LAMR1-TP1 binding protein (RVAP27). We metabolically labeled 2.0×10^5 COS7 cells expressing either PCDNA3.1-Myc-tagged-Lamr1 or PCDNA3.1-Myc-tagged-Lamr1-tp1 (Invitrogen) with ^{35}S, lysed them with 1 ml of lysis buffer (20 mM Tris pH 8.0, 5% acetonitrile, 5 M MEDTA, 1% Nonidet P-40) and immunoprecipitated them with a Myc antibody. Bound materials were separated by SDS-PAGE and the radioactivity was detected by a BAS imaging analyzer (Fuji). The eluted fraction from Myc-antibody beads was also injected onto a Phenyl-RPLC column (4.6 × 250mm, Nakarai) equilibrated with 0.1% trifluoroacetic acid and 5% acetonitrile. Fractions were eluted with a linear gradient of 27–37% acetonitrile at a flow rate of 1 ml. Each fraction was lyophilized and separated by SDS-PAGE. Radioactivity was detected by BAS imaging system.

Large-scale purification and sequence analysis of LAMR1-TP1–binding protein. COS7 cells (1.0×10^8) expressing Myc-tagged LAMR1-TP1 were lysed with 200 ml of lysis buffer and applied to 500 µl of Myc-antibody beads (Clontech). Bound materials were eluted with 0.1% trifluoroacetic acid and 5% acetonitrile. The eluted fraction was diluted 50 times with a lysis buffer and was applied to Uno-Q anion exchange column (Bio-Rad). The column was equilibrated with 20 mM Tris and 5% acetonitrile at pH 8.0 and bound materials were eluted with a linear gradient of NaCl (0–0.5 M) at a flow rate of 1 ml min^{-1}. Five fractions of about 0.3 M NaCl elution were pooled and injected onto a Phenyl-RPLC column (4.6 × 250 mm, Nakarai) equilibrated with 0.1% trifluoroacetic acid and 5% acetonitrile. Fractions were eluted with a linear gradient of 27–37% acetonitrile at a flow rate of 1 ml. After separating by SDS-PAGE, RVAP27 was eluted at the same fraction in which the radioactive LAMR1-TP1 was detected. Purified RVAP (10 pmol) was subjected to SDS-PAGE on 12% gel. After staining the gel with SyproRuby, the 27-kDa band was cut and treated with trypsin. The tryptic digest was fractionated by nanoscale HPLC on a C18 column (0.1 × 50 mm). Two fractions were analyzed by direct N-terminal sequence by Edman degradation with the HP G1005 Protein Sequencing System. One fraction was analyzed with a tandem mass spectrometer (Q-Tof2) equipped with a nanoelectrospray ionization source. Positive ion tandem mass spectra were measured.

RNA preparation and hybridization to oligonucleotide arrays. Total RNA was isolated from viable mice or cultured neonatal cardiomyocytes derived from C57Bl/6 mice. Affymetrix Gene Chip technology was used as described[36]. Briefly, cDNA was synthesized from total RNA and annealed to a T7-oligo-dT primer. Reverse transcription was done with Superscript II reverse transcriptase. Second-strand cDNA synthesis was done with DNA polymerase I with the appropriate reagents. Synthesis of biotin-labeled cRNA was done by *in vitro* transcription with the MEGAscript T7 IVT Kit (Ambion, Inc). The cRNA was fragmented and hybridized to GeneChip Murine U74vA2 Array Set (Affymetrix). Hybridization, probe washing, staining and probe array scan were done according to the protocols provided by Affymetrix. Detailed information about the array protocol and data is available in the GEO database (see URL and accession number below).

Real-time PCR. Real-time PCR was done with TaqMan technology and the ABI Prism 7700 Detection System (Applied Biosystems). Reactions (25 µl) were set up using the 2× Universal PCR Master Mix (Applied Biosystems), template cDNA and adequate concentrations of primers and probes. All of the samples were processed in duplicate. To standardize the quantity of the two selected genes, GAPDH was used as the endogenous control reference because our microarray analysis showed that the level of GAPDH was stable and no significant difference was noted among all the three groups.

Data analysis. GeneSpring 5.0 (Silicon Genetics) software was used for analyses. A global normalization was used for all data in the 18 arrays with a combination of three steps: transforming negative values to 0.01, normalizing to the 50th percentile per chip and normalizing to median per gene. We filtered data using a combination of signal confidence ('present' flag), relative change (1.5–2.0 times), minimum acceptable signal intensity (average difference ≥50 in at least one of three groups) and a statistical cut-off ($P < 0.05$, Student's *t*-test). Data are presented as mean or mean ± s.e.m.; the one-way ANOVA with Tukey-Kramer exact probability test was used to test the differences among all the groups and the least-squares method was used to determine linear correlation between selected variables. $P < 0.05$ was considered statistically significant.

Animal experiments. All animal experiments were approved by the Institutional Animal Care and Use Committee at Osaka University Graduate School of Medicine.

URL. The GEO database is available at http://www.ncbi.nlm.nih.gov/geo/.

GEO accession number. GSE927.

Note: Supplementary information is available on the Nature Genetics website.

ACKNOWLEDGMENTS

These data were generated through the use of the Celera Discovery System and Celera Genomics' Associated Databases. We thank T. Tanaka and K. Miyake for assistance with DNA sequencing; S. Hirota for histologic expertise; H. Niwa for donating plasmid constructs and providing suggestions; K. Yamamoto for amino-acid sequencing; and H. Kikutani, K. Node and T. Nakagawa for discussions. This work was supported by Grants-in-aid for Scientific Research from the Japanese Ministry of Education, Culture, Sports, Science and Technology and from the Ministry of Health and Labor and Welfare, Japan.

COMPETING INTERESTS STATEMENT

The authors declare that they have no competing financial interests.

Received 20 November; accepted 29 December 2003
Published online at http://www.nature.com/naturegenetics/

1. Thiene, G. *et al.* Arrythmogenic right ventricular cardiomyopathy. *Trends Cardiovasc. Med.* **7**, 84–90 (1997).
2. Severini, G.M. *et al.* A new locus for arrhythmogenic right ventricular dysplasia on the long arm of chromosome 14. *Genomics* **31**, 193–200 (1996).
3. Rampazzo, A. *et al.* ARVD4, a new locus for arrhythmogenic right ventricular cardiomyopathy, maps to chromosome 2 long arm. *Genomics* **45**, 259–263 (1997).
4. Ahmad, F. *et al.* Localization of a gene responsible for arrhythmogenic right ventricular dysplasia to chromosome 3p23. *Circulation* **98**, 2791–2795 (1998).
5. Li, D. *et al.* The locus of a novel gene responsible for arrhythmogenic right- ventricular dysplasia characterized by early onset and high penetrance maps to chromosome 10p12-p14. *Am. J. Hum. Genet.* **66**, 148–156 (2000).
6. Tiso, N. *et al.* Identification of mutations in the cardiac ryanodine receptor gene in families affected with arrhythmogenic right ventricular cardiomyopathy type 2 (ARVD2). *Hum. Mol. Genet.* **10**, 189–194 (2001).
7. Bright, J.M. & McEntee, M. Isolated right ventricular cardiomyopathy in a dog. *J. Am. Vet. Med. Assoc.* **207**, 64–66 (1995).
8. Simpson, K.W., Bonagura, J.D. & Eaton, K.A. Right ventricular cardiomyopathy in a dog. *J. Vet. Intern. Med.* **8**, 306–309 (1994).
9. Fox, P.R., Maron, B.J., Basso, C., Liu, S.K. & Thiene, G. Spontaneously occurring arrhythmogenic right ventricular cardiomyopathy in the domestic cat: A new animal model similar to the human disease. *Circulation* **102**, 1863–1870 (2000).
10. Ishikawa, S., Zu Rhein, G.M. & Gilbert, E.F. Uhl's anomaly in the mink. Partial absence of the right atrial and ventricular myocardium. *Arch. Pathol. Lab. Med.* **101**, 388–390 (1977).
11. Sato, M. *et al.* Analysis of nuclear localization of laminin binding protein precursor p40 (LBP/p40). *Biochem. Biophys. Res. Commun.* **229**, 896–901 (1996).
12. Kaneda, Y. *et al.* The induction of apoptosis in HeLa cells by the loss of LBP-p40. *Cell Death Differ.* **5**, 20–28 (1998).
13. Kondo, K., Nozawa, K., Tomita, T. & Ezaki, K. Inbred strains resulting from Japanese mice. *Bull. Exp. Anim.* **6**, 107–112 (1967).
14. Nakamura, M. & Yamada, K. Studies on a diabetic (KK) strain of the mouse. *Diabetologia* **3**, 212–221 (1967).
15. McKenna, W.J. *et al.* Diagnosis of arrhythmogenic right ventricular dysplasia/cardiomyopathy. Task Force of the Working Group Myocardial and Pericardial Disease of the European Society of Cardiology and of the Scientific Council on Cardiomyopathies of the International Society and Federation of Cardiology. *Br. Heart J.* **71**, 215–218 (1994).
16. Lin, H., Parmacek, M.S., Morle, G., Bolling, S. & Leiden, J.M. Expression of recombinant genes in myocardium in vivo after direct injection of DNA. *Circulation* **82**, 2217–2221 (1990).
17. Nakayama, J., Rice, J.C., Strahl, B.D., Allis, C.D. & Grewal, S.I. Role of histone H3 lysine 9 methylation in epigenetic control of heterochromatin assembly. *Science* **292**, 110–113 (2001).
18. Festenstein, R. *et al.* Modulation of heterochromatin protein 1 dynamics in primary Mammalian cells. *Science* **299**, 719–721 (2003).
19. Cranefield, P. *The Conduction of the Cardiac Impulse* (Futura, Mount Kisco, New York, 1975).
20. Peters, S. & Trummel, M. Diagnosis of arrhythmogenic right ventricular dysplasia-cardiomyopathy: value of standard ECG revisited. *Ann. Noninvasive Electrocardiol.* **8**, 238–245 (2003).

21. Nasir, K. *et al.* Filtered QRS duration on signal-averaged electrocardiography predicts inducibility of ventricular tachycardia in arrhythmogenic right ventricle dysplasia. *Pacing Clin. Electrophysiol.* **26**, 1955–1960 (2003).
22. Burke, A.P., Farb, A., Tashko, G. & Virmani, R. Arrhythmogenic right ventricular cardiomyopathy and fatty replacement of the right ventricular myocardium: are they different diseases? *Circulation* **97**, 1571–1580 (1998).
23. Protonotarios, N. *et al.* Genotype-phenotype assessment in autosomal recessive arrhythmogenic right ventricular cardiomyopathy (Naxos disease) caused by a deletion in plakoglobin. *J. Am. Coll. Cardiol.* **38**, 1477–1484 (2001).
24. Steenman, M. *et al.* Transcriptomal analysis of failing and nonfailing human hearts. *Physiol. Genomics* **12**, 97–112 (2003).
25. Pashmforoush, M. *et al.* Adult mice deficient in actinin-associated LIM-domain protein reveal a developmental pathway for right ventricular cardiomyopathy. *Nat. Med.* **7**, 591–597 (2001).
26. Cheutin, T. *et al.* Maintenance of stable heterochromatin domains by dynamic HP1 binding. *Science* **299**, 721–725 (2003).
27. Zhang, C.L. *et al.* Class II histone deacetylases act as signal-responsive repressors of cardiac hypertrophy. *Cell* **110**, 479–488 (2002).
28. Zhang, C.L., McKinsey, T.A. & Olson, E.N. Association of class II histone deacetylases with heterochromatin protein 1: potential role for histone methylation in control of muscle differentiation. *Mol. Cell. Biol.* **22**, 7302–7312 (2002).
29. McCarrey, J.R. & Thomas, K. Human testis-specific PGK gene lacks introns and possesses characteristics of a processed gene. *Nature* **326**, 501–505 (1987).
30. Gebara, M.M. & McCarrey, J.R. Protein-DNA interactions associated with the onset of testis-specific expression of the mammalian Pgk-2 gene. *Mol. Cell. Biol.* **12**, 1422–1431 (1992).
31. Dahl, H.H., Brown, R.M., Hutchison, W.M., Maragos, C. & Brown, G.K. A testis-specific form of the human pyruvate dehydrogenase E1 α subunit is coded for by an intronless gene on chromosome 4. *Genomics* **8**, 225–232 (1990).
32. Hirotsune, S. *et al.* An expressed pseudogene regulates the messenger-RNA stability of its homologous coding gene. *Nature* **423**, 91–96 (2003).
33. Richardson, M.P., Braybrook, C., Tham, M., Moore, G.E. & Stanier, P. Molecular cloning and characterization of a highly conserved human 67- kDa laminin receptor pseudogene mapping to Xq21.3. *Gene* **206**, 145–150 (1998).
34. Gordon, J.W., Scangos, G.A., Plotkin, D.J., Barbosa, J.A. & Ruddle, F.H. Genetic transformation of mouse embryos by microinjection of purified DNA. *Proc. Natl. Acad. Sci. USA* **77**, 7380–7384 (1980).
35. Simpson, P., McGrath, A. & Savion, S. Myocyte hypertrophy in neonatal rat heart cultures and its regulation by serum and by catecholamines. *Circ. Res.* **51**, 787–801 (1982).
36. Lockhart, D.J. *et al.* Expression monitoring by hybridization to high-density oligonucleotide arrays. *Nat. Biotechnol.* **14**, 1675–1680 (1996).

Available online at www.sciencedirect.com
SCIENCE DIRECT®
Biochemical and Biophysical Research Communications 320 (2004) 376–382
BBRC
www.elsevier.com/locate/ybbrc

Roles of charged amino acid residues in the cytoplasmic domain of proHB-EGF

Daisuke Nanba,[a] Fujio Toki,[a,b] and Shigeki Higashiyama[a,c,*]

[a] *Division of Biochemistry and Molecular Genetics, Department of Molecular and Cellular Biology, Ehime University School of Medicine, Shitsukawa, Shigenobu-cho, Onsen-gun, Ehime 791-0295, Japan*
[b] *Department of Molecular Pathology, School of Allied Health Sciences, Osaka University, Suita, Osaka 565-0871, Japan*
[c] *PRESTO, JST, Japan*

Received 6 May 2004
Available online 15 June 2004

Abstract

Heparin-binding EGF-like growth factor (HB-EGF) is initially synthesized as a type I transmembrane precursor (proHB-EGF). Proteolytic cleavage of proHB-EGF yields amino- and carboxy-terminal fragments (HB-EGF and HB-EGF-C, respectively). We have previously shown that HB-EGF-C is translocated from the plasma membrane into the nucleus, where it interacts with the transcription repressor, PLZF. Here we characterize the amino acid residues of the cytoplasmic domain of proHB-EGF on cell surface distribution and the interaction of HB-EGF-C with PLZF. The cytoplasmic domain contains three characteristic clusters with charged amino acids. Generation of various mutants of proHB-EGF showed that the arrangement of the charged amino acids in the cytoplasmic domain regulates the distribution of proHB-EGF at the plasma membrane but does not regulate proHB-EGF processing and internalization of HB-EGF-C. Further, the charged amino acids are also required for HB-EGF-C–PLZF interaction. These results indicate that the cytoplasmic domain of proHB-EGF is a multifunctional domain.

Keywords: HB-EGF; PLZF; EGF family; Intracellular signaling; Membrane-anchored growth factor

Heparin-binding EGF-like growth factor (HB-EGF) is a member of the EGF family that was first identified as a secreted product of macrophages and macrophage-like U-937 cells [1]. It is a 20–22 kDa glycoprotein found in multiple forms of 76–86 amino acids [2]. HB-EGF binds directly to the EGF receptor (EGFR)/ErbB1 [1] and ErbB4 [3], activates ErbB2 indirectly by receptor heterodimerization [4], and induces ErbBs signaling in cells. *N*-Arginine dibasic convertase (NRDc) has been also identified as a specific cell surface receptor for HB-EGF that enhances cell migration in response to HB-EGF via EGFR [5].

A structural feature common to all members of the EGF family is their synthesis via a precursor molecule that is tethered to the plasma membrane via a transmembrane domain [6]. Before HB-EGF is secreted by cells, it is processed from a 208 amino acid precursor composed of various domains (e.g., signal peptide, propeptide, heparin-binding, EGF-like, transmembrane, and cytoplasmic) [1,2]. The membrane-anchored precursor of HB-EGF (proHB-EGF) exerts its bioactivity in two distinct ways: it serves a receptor for diphtheria toxin [7], a specific function not shared by other EGF family members [8,9], and it stimulates growth of adjacent cells [10].

Newly synthesized proHB-EGF molecules first undergo amino-terminal processing at Arg^{62}-Asp^{63} by the endoprotease, furin [11]. Next, cleavage at a Pro^{149}-Val^{150} by "a disintegrin and metalloprotease" (ADAM) molecules and matrix metalloproteases [12,13] takes place to release a soluble form of HB-EGF. This cleavage can be stimulated by various regents, including the phorbol ester 12-*O*-tetradecanoylphorbol-13-acetate (TPA) [14]. The processing of the extracellular domain, which is termed "ectodomain shedding," also creates a

* Corresponding author. Fax: +81-89-960-5256.
E-mail address: shigeki@m.ehime-u.ac.jp (S. Higashiyama).

0006-291X/$ - see front matter © 2004 Elsevier Inc. All rights reserved.
doi:10.1016/j.bbrc.2004.05.176

remnant carboxy-terminal cell-associated fragment (HB-EGF-C) consisting of juxtamembrane, transmembrane, and cytoplasmic domains.

We recently reported that HB-EGF-C interacts with a nuclear transcriptional repressor, promyelocytic leukemia zinc finger (PLZF), and evokes a novel intracellular signaling pathway that is independent of EGFR activation [15]. HB-EGF-C–PLZF interaction is mediated by the cytoplasmic domain of proHB-EGF. In addition, neuregulin-1, a member of the family of EGF molecules, is cleaved at the transmembrane domain. The intracellular domain (Nrg-1-ICD) released from this process regulates gene transcription [16]. These findings indicate that the cytoplasmic domain of the membrane-anchored precursor of the EGF family molecules is a functional domain.

Here we characterize amino acid residues of the cytoplasmic domain for the distribution of proHB-EGF on cell surface and the interaction of HB-EGF-C with PLZF. The specific sequences of amino acid residues of the cytoplasmic domain were required for proHB-EGF distribution at plasma membrane and the interaction of HB-EGF-C with PLZF after proHB-EGF processing. These results indicate that the cytoplasmic tail of proHB-EGF is a multifunctional domain.

Materials and methods

Plasmid construction. Plasmids for recombinant expression of YFP-tagged proHB-EGF, CFP-tagged PLZF, and FLAG-tagged PLZF were described previously [15]. DNA fragments encoding the deleted or mutant cytoplasmic region of proHB-EGF (with or without the stop codon deleted) were generated by PCR and substituted for the corresponding region of pEYFP-N1-proHB-EGF [15]. Plasmids for recombinant expression of GST-fused HB-TMC and HB-TMCM were generated by subcloning the *Bam*HI–*Eco*RI fragment containing the transmembrane and cytoplasmic domain sequence made by PCR at the *Bam*HI/*Eco*RI sites of pGEX6P-1 (Amersham Biosciences). All cDNA constructs were purified by QIAGEN Plasmid Maxi kit and verified by DNA sequence.

Cell lines and transfection. Preparation and maintenance of HT1080/proHB-EGF cells was described previously [15]. For the establishment of HT1080/proHBcytoM cells, the plasmids encoding proHBcytoM mutants were introduced into HT1080 cells using Lipofectamine 2000 (Invitrogen), and stably transfected clones were isolated. HT1080 cells were grown in Eagle-MEM supplemented with non-essential amino acids (Invitrogen), 10% fetal bovine serum (FBS), and antibiotics. Stable transfectants were maintained in the same medium with 1 mg/ml G418. All cells were cultured in a humidified 37 °C/5% CO_2 incubator.

For transient transfections, 4.0×10^5 cells were seeded in 35-mm cell-culture dishes (CORNING), grown for 12 h in medium, and then transfected with expression vectors using Lipofectamine 2000 (Invitrogen).

Immunoblotting. Immunoblotting was performed as described previously [14]. Primary antibodies were used as follows: rabbit polyclonal antibody to GFP (MBL International Corporation) and mouse monoclonal antibody to FLAG (Sigma–Aldrich). Secondary antibodies were HRP-conjugated goat anti-mouse and rabbit IgG.

Imaging of YFP- and CFP-tagged protein and immunofluorescence microscopy. The assessment of subcellular localization of YFP- or CFP-fusion proteins and immunofluorescence microscopy were performed as described previously [15]. The following primary antibodies were used: a goat polyclonal antibody to clathrin (Sigma–Aldrich) and a mouse monoclonal antibody to caveolin-1 (BD Transduction Laboratories). The following secondary antibodies were used: rhodamine-conjugated donkey anti-goat IgG and rhodamine-conjugated goat anti-mouse IgG (CHEMICON). Some cells were also stained with Hoechst 33258 (Molecular probes)

GST pull-down assay. GST, GST-HB-TMC, and GST-HB-TMCM were expressed in and purified from the *E. coli* BL21 strain according to standard protocol. GST pull-down assay was performed as previously described [15].

Results

Cytoplasmic structure of proHB-EGF

The cytoplasmic domain of proHB-EGF consists of 24 amino acids with three characteristic clusters of charged amino acid residues; the first is a positively charged cluster (RYHRR), the second is a negatively charged cluster (DVENEE), and the third is a positively charged cluster (KVK) (Figs. 1A and 2A).

Processing and distribution of proHB-EGF truncated mutants

Recombinant protein in which YFP was fused to the carboxy-terminus of proHB-EGF (proHB-EGF~YFP) was synthesized as an expected size, distributed at the plasma membrane, and proteolytically cleaved after TPA treatment (Figs. 1B and C). To investigate the role of the cytoplasmic domain on proHB-EGF processing and subcellular localization, we first constructed plasmids encoding three types of YFP-tagged cytoplasmic deletion mutants of proHB-EGF (proHBΔC10~YFP, proHBΔC19~YFP, and proHBΔC22~YFP; Fig. 1A). These expression plasmids were transiently transfected into human fibrosarcoma HT1080 cells, and the fusion proteins were detected by immunoblotting using anti-GFP antibody after the treatment with or without 100 nM TPA for 60 min. All YFP fusion proteins were detected as heterogeneous bands at ~49 and ~36 kDa, respectively (Fig. 1B). Pro-forms of these recombinant proteins were detected as ~49 kDa bands in each lane. After TPA stimulation, carboxy-terminal fragments of these pro-forms were detected as ~36 kDa bands in each lane. TPA treatment decreased the intensity of the ~49 kDa bands in the three types of the truncated mutants as well as in proHB-EGF~YFP. This suggests that these truncated mutants are processed normally in response to TPA stimulation.

The distribution of YFP-fusion proHB-EGF variants was assessed using a fluorescent microscope. In the absence of TPA, all fusions were mainly localized at the plasma membrane. While proHB-EGF~YFP and proHBΔC10~YFP were distributed homogeneously throughout the plasma membrane, cells expressing

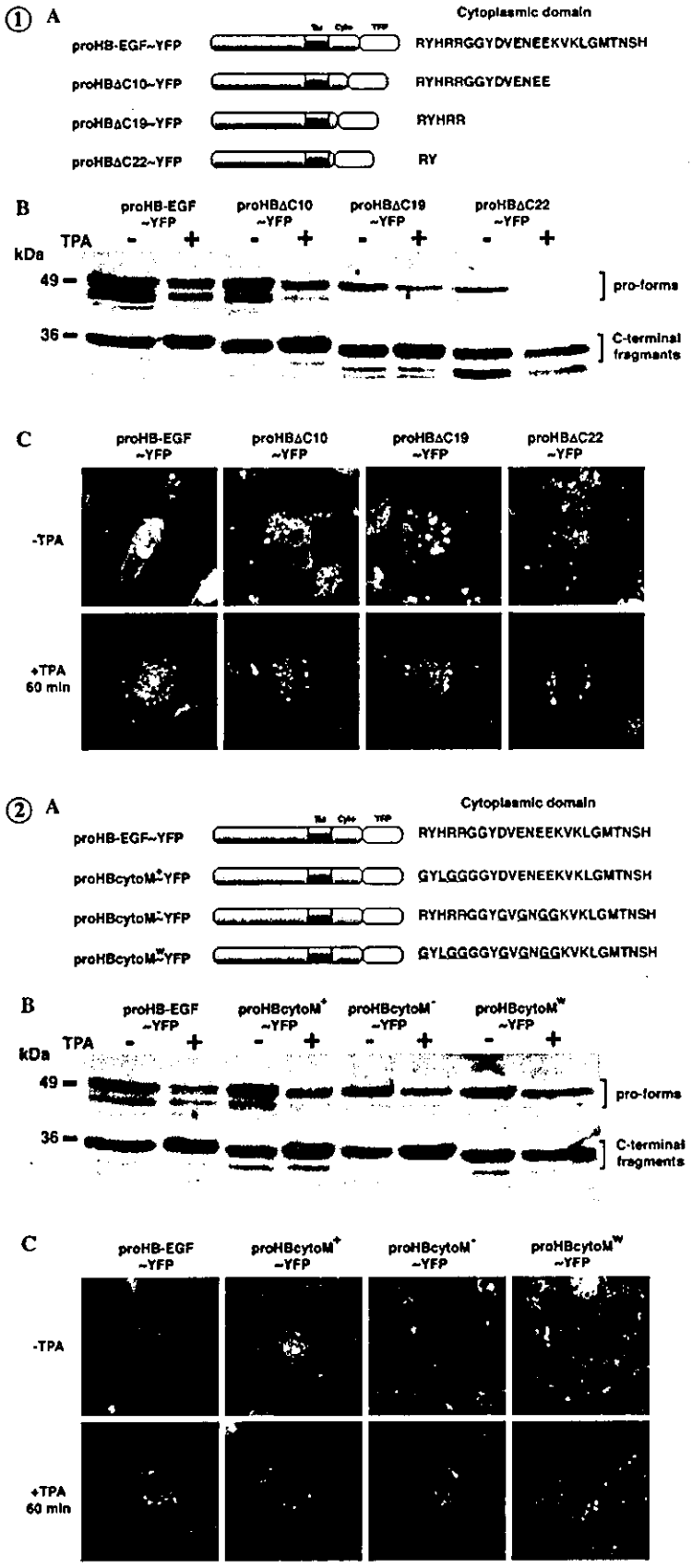
① A
Cytoplasmic domain
proHB-EGF~YFP
RYHRRGGYDVENEEKVKLGMTNSH
proHBΔC10~YFP
RYHRRGGYDVENEE
proHBΔC19~YFP
RYHRR
proHBΔC22~YFP
RY
B
proHB-EGF ~YFP
proHBΔC10 ~YFP
proHBΔC19 ~YFP
proHBΔC22 ~YFP
TPA
kDa
49
36
pro-forms
C-terminal fragments
C
-TPA
+TPA 60 min
② A
Cytoplasmic domain
proHB-EGF~YFP
RYHRRGGYDVENEEKVKLGMTNSH
proHBcytoM+~YFP
GYLGGGGYDVENEEKVKLGMTNSH
proHBcytoM-~YFP
RYHRRGGYGVGNGGKVKLGMTNSH
proHBcytoMW~YFP
GYLGGGGYGVGNGGKVKLGMTNSH
B
proHB-EGF ~YFP
proHBcytoM+ ~YFP
proHBcytoM- ~YFP
proHBcytoMW ~YFP
TPA
kDa
49
36
pro-forms
C-terminal fragments
C
-TPA
+TPA 60 min

proHBΔC19~YFP and proHBΔC22~YFP had patches of the YFP-fusion proteins at the plasma membrane (Fig. 1C). After TPA treatment, the carboxy-terminal fragments of all fusion proteins were localized around the nucleus (Fig. 1C).

Processing and distribution of proHB-EGF cytoplasmic uncharged mutants

The proHB-EGF cytoplasmic domain contains three clusters of charged amino acids (Fig. 2A). To investigate the roles of these charged clusters, we generated three types of proHB-EGF~YFP uncharged mutants by replacing clusters of charged amino acids with those of uncharged amino acids (proHBcytoM$^+$~YFP and proHBcytoM$^-$~YFP, and proHBcytoM^w~YFP; Fig. 2A). The plasmids encoding proHB-EGF~YFP and three types of uncharged mutants were transiently transfected into HT1080 cells, and the recombinant proteins were detected by immunoblotting with an anti-GFP antibody after incubation in medium with or without TPA. All three mutant proteins and proHB-EGF~YFP underwent normal processing in response to TPA stimulation (Fig. 2B).

The subcellular localization of recombinant YFP fusion was assessed under a fluorescent microscope. When the transfected cells were incubated with normal medium, proHB-EGF~YFP was distributed homogeneously throughout the plasma membrane. In contrast, cells transfected with three types of mutants showed patch-like distribution of YFP-fused mutant proteins (Fig. 2C). Following treatment with TPA, the cells expressing proHB-EGF~YFP and its mutants showed carboxy-terminal fragments distribution around the nucleus (Fig. 2C).

HB-EGF-C internalization is mediated by clathrin-dependent endocytosis

The images of truncated mutants of proHB-EGF~YFP after TPA treatment indicate that the cytoplasmic domain is not necessary for the internalization of HB-EGF-C. HB-EGF-C retains the transmembrane domain [15] and, therefore, can be carried into the cytoplasm by a vesicle trafficking mechanism, such as clathrin- and caveolin-mediated endocytosis. To test this possibility, we performed immunostaining with antibodies against clathrin and caveolin-1 in HT1080 cells transiently expressing proHB-EGF~YFP. ProHB-EGF~YFP was localized to the plasma membrane. After TPA treatment for 30 min, the carboxy-terminal fragments of proHB-EGF~YFP (HB-EGF-C~YFP) were localized around the nucleus. In this condition, HB-EGF-C~YFP co-localized with clathrin but not with caveolin-1 (Figs. 3A and B). These results indicate that HB-EGF-C containing the transmembrane domain is internalized into the cytoplasm by a process that is at least partially dependent on clathrin-mediated endocytosis.

Charged amino acid residues in the cytoplasmic domain of proHB-EGF are essential for PLZF export induced by proHB-EGF processing

We have previously reported that the cytoplasmic domain of proHB-EGF is required for PLZF export from the nucleus [15]. To investigate the effect of charged amino acid clusters in the cytoplasmic domain, we established HT1080 cells stably expressing proHB-EGF, proHBcytoM$^+$, proHBcytoM$^-$, and proHBcytoM^w (Fig. 4A). The plasmid for recombinant expression of CFP~PLZF was transiently transfected into HT1080 cells and its variants, and images of the CFP-fusion protein were collected with or without the treatment with 100 nM TPA for 60 min. In all cell types, CFP~PLZF was predominantly localized at the nucleus before TPA stimulation (Figs. 4B and C). TPA treatment resulted in distribution of CFP~PLZF throughout the entire cytoplasm of HT1080/proHB-EGF cells (Figs. 4B and C), as previously reported [15]. In HT1080/proHBcytoM$^+$ and HT1080/proHBcytoM$^-$ cells, however, the nuclear export of CFP~PLZF after TPA treatment was partially inhibited (Figs. 4B and C). Furthermore, in HT1080/

Fig. 1. Processing and distribution of proHB-EGF truncated mutants. (A) Schematic structure of proHB-EGF~YFP truncated mutants. (B) Expression of YFP-fusion proteins was detected by immunoblotting with anti-GFP antibody. The ~49 kDa band of pro-form of each YFP-fusion protein was decreased by the TPA stimulation. In contrast, the ~36 kDa band of the carboxy-terminal fragment from each YFP-fusion pro-form (C-terminal fragment) was increased after the treatment. (C) Distribution of YFP-fusion proteins (green) and nucleus (blue). ProHB-EGF~YFP and proHBΔC10~YFP were distributed homogeneously throughout the plasma membrane, while proHBΔC19~YFP and proHBΔC22~YFP showed patch-like distribution in the plasma membrane. The carboxy-terminal fragments of proHB-EGF~YFP and its variants generated by the TPA treatment were localized around the nucleus. Bar = 10 μm.

Fig. 2. Processing and distribution of proHB-EGF cytoplasmic uncharged mutants. (A) Schematic structure of proHB-EGF~YFP cytoplasmic uncharged mutants. (B) Expression of YFP-fusion proteins was detected by immunoblotting with anti-GFP antibody. The band of pro-form of each YFP-fusion protein decreased in response to TPA stimulation. In contrast, the band of the carboxy-terminal fragment of each YFP-fusion pro-form (C-terminal fragment) increased in response to treatment. (C) Distribution of YFP-fusion proteins (green) and nucleus (blue). ProHB-EGF~YFP was distributed homogeneously throughout the plasma membrane, while the three types of cytoplasmic uncharged mutants were distributed in a patch-like fashion in the plasma membrane. The carboxy-terminal fragments of proHB-EGF~YFP and its variants generated by the TPA treatment were localized around the nucleus. Bar = 10 μm.

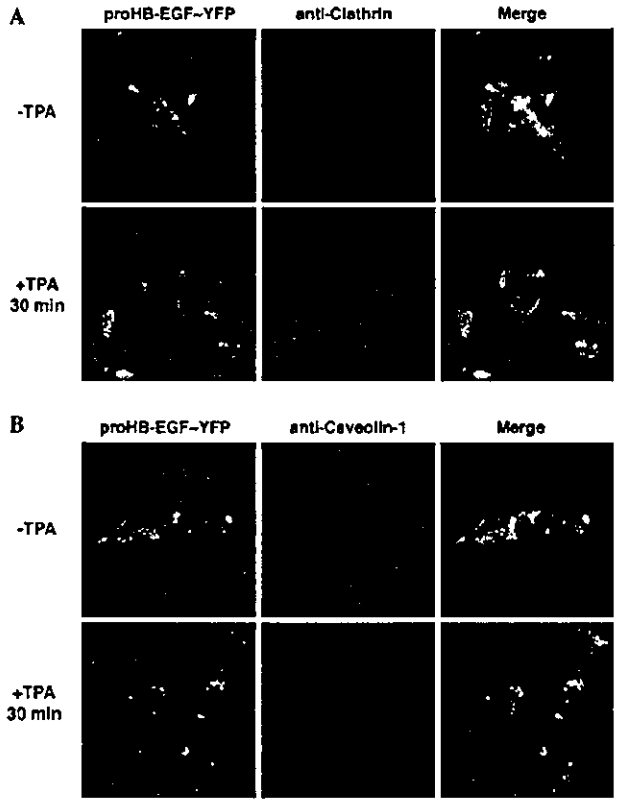

Fig. 3. Colocalization of the carboxy-terminal fragment of proHB-EGF~YFP (HB-EGF-C~YFP) with clathrin following TPA treatment. (A,B) HT1080 cells transiently expressing proHB-EGF~YFP were immunostained with anti-clathrin and caveolin-1 antibodies, respectively, before and after TPA stimulation. (A) After the treatment, HB-EGF-C~YFP colocalized with clathrin around the nucleus. (B) Colocalization of HB-EGF-C~YFP with caveolin-1 was not observed following TPA treatment. Bars = 10 μm.

proHBcytoM^{w} cells, the degree of PLZF export was greatly reduced (Figs. 4B and C).

Sequence specific required for interaction of HB-EGF-C with PLZF

Interaction between PLZF and HB-EGF-C is required for PLZF export [15]. We investigated the binding of PLZF with HB-EGF-C containing wild-type- or an uncharged mutant cytoplasmic domain using a GST pull-down assay. Glutathione–Sepharose beads conjugated either with GST alone, with recombinant fragments containing transmembrane and cytoplasmic domain of proHB-EGF fused to GST (GST-HB-TMC), or with recombinant fragments containing transmembrane and uncharged mutant cytoplasmic domain fused to GST (GST-HB-TMCM) (Figs. 5A and B) were generated. Next, cell lysate containing FLAG-tagged PLZF was incubated with these beads. PLZF associated with GST-HB-TMC, but not with GST alone or with GST-HB-TMCM (Fig. 5C).

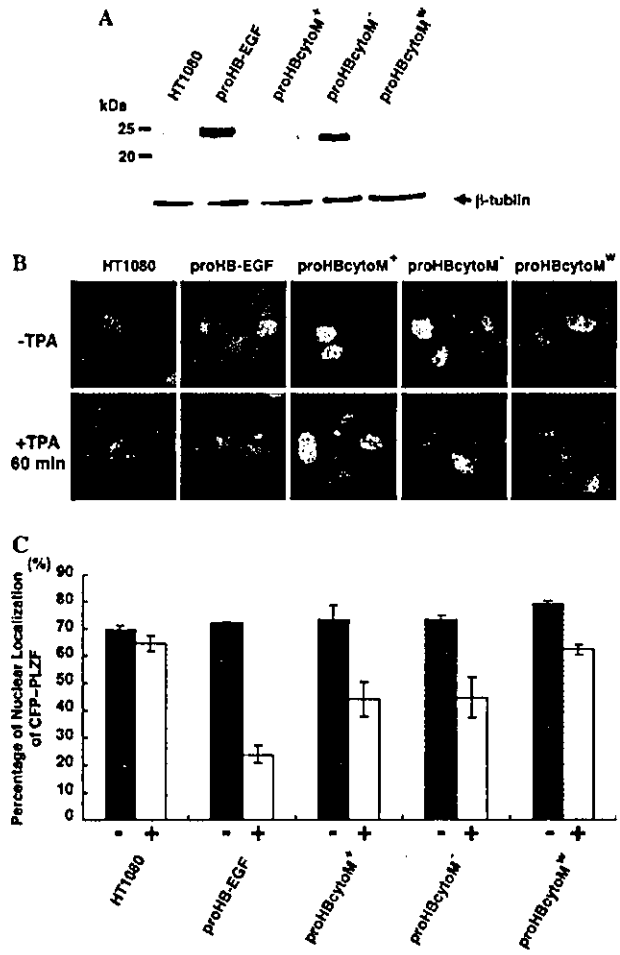

Fig. 4. ProHB-EGF processing-dependent nuclear export of PLZF requires charged clusters in the cytoplasmic domain of proHB-EGF. (A) HT1080 cells stably expressing proHB-EGF, proHBcytoM^{+}, proHBcytoM^{-}, and proHBcytoM^{w} were established. Expression of proHB-EGF and its variants confirmed by immunoblotting with anti-HB-EGF antibody (upper panel). The expression of β-tubulin was used as control (lower panel). (B,C) Subcellular localization of CFP~PLZF fusion protein in HT1080 cells and its variants. CFP~PLZF expression vector was transiently transfected into HT1080 cells and its transfectants. CFP~PLZF was predominantly localized to the nucleus in these cell types. In HT1080/proHB-EGF but not in parental HT1080 cells, CFP~PLZF was distributed in the entire cytoplasm following treatment with 100 nM TPA. In HT1080/proHBcytoM^{+} and HT1080/proHBcytoM^{-} cells, the nuclear export of CFP~PLZF was partially inhibited. The degree of CFP~PLZF export was greatly decreased in HT1080/proHBcytoM^{w} cells.

Discussion

We have previously shown that HB-EGF-C is translocated from the plasma membrane to the nucleus after proHB-EGF processing and that HB-EGF-C interacts with PLZF [15]. The present study demonstrated that the cytoplasmic domain of proHB-EGF plays a key role in proHB-EGF distribution and HB-EGF-C–PLZF interaction.

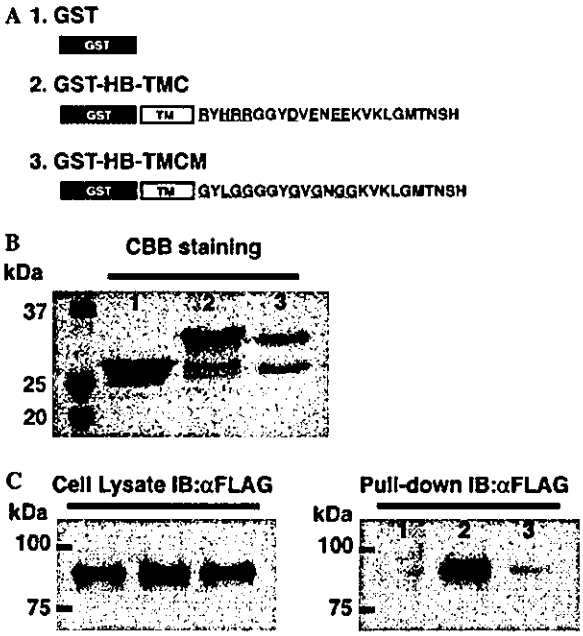

Fig. 5. Sequence specific interaction of the cytoplasmic domain of proHB-EGF with PLZF. (A) Schematic structures of GST alone, GST-HB-TMC, and GST-HB-TMCM. (B) GST (1), GST-HB-TMC (2), or GST-HB-TMCM (3) separated by SDS–PAGE were stained with CBB. (C) Cell lysates containing FLAG-tagged PLZF were incubated with GST (1), GST-HB-TMC (2), or GST-HB-TMCM (3) beads, and bound proteins were detected by immunoblotting with anti-FLAG antibody (right panel). Expression of FLAG-tagged PLZF was confirmed by immunoblotting using anti-FLAG antibody (left panel). FLAG-tagged PLZF was bound to GST-HB-TMC but not to GST alone or to GST-HB-TMCM.

In the present study we demonstrated that the cytoplasmic domain of proHB-EGF was not required for the proteolytic processing of proHB-EGF. This result is consistent with the report that the processing of precursors of HB-EGF and amphiregulin occurred in the absence of their cytoplasmic domain [17,18]. In this study, proHBΔC19~YFP and proHBΔC22~YFP showed patch-like distribution at the plasma membrane. In addition, cells transiently expressing three types of uncharged cytoplasmic mutants of proHB-EGF~YFP showed a similar type of distribution. These results indicate that the arrangement of the first positively and the second negatively charged clusters in the cytoplasmic domain is required for proper distribution of proHB-EGF at the plasma membrane.

The nuclear export of PLZF is dependent on proHB-EGF processing and requires the cytoplasmic domain of proHB-EGF [15]. Further, the present study demonstrated that the characteristic sequence of charged amino acid residues in the cytoplasmic domain of proHB-EGF was essential for interaction with PLZF and its subsequent nuclear export, but was not required for the translocation of HB-EGF-C. The presence of a transmembrane domain in HB-EGF-C [15] and colocalization of HB-EGF-C with clathrin indicate that the internalization of HB-EGF-C is at least partially mediated by clathrin-dependent endocytosis. Precursors of other EGF family members also possess charged amino acid clusters in their cytoplasmic domains, suggesting that their carboxy-terminal fragments of their pro-forms can interact with PLZF or similar transcription repressors after their processing.

In conclusion, the cytoplasmic domain of proHB-EGF regulates proHB-EGF distribution at the plasma membrane, and the arrangement of charged amino acid clusters in the cytoplasmic domain is essential for HB-EGF-C–PLZF interaction. These results indicate that the cytoplasmic domain is a multifunctional domain. Focusing on the cytoplasmic domain of proHB-EGF and other EGF family precursors may be useful in the characterization of the functional diversity of EGF family molecules.

Acknowledgments

This study is supported by Grants-in-Aid for Scientific Research (Nos. 13670139, 13216057, and 15390097) to S. Higashiyama from the Ministry of Education, Science and Culture, Japan, and in part by Uehara Memorial Foundation and The Sumitomo Foundation.

References

[1] S. Higashiyama, J.A. Abraham, J. Miller, J.C. Fiddes, M. Klagsbrun, A heparin-binding growth factor secreted by macrophage-like cells that is related to EGF, Science 251 (1991) 936–939.
[2] S. Higashiyama, K. Lau, G.E. Besner, J.A. Abraham, M. Klagsbrun, Structure of heparin-binding EGF-like growth factor: multiple forms, primary structure, and glycosylation of the mature protein, J. Biol. Chem. 267 (1992) 6205–6212.
[3] K. Elenius, S. Paul, G. Allison, J. Sun, M. Klagsbrun, Activation of HER4 by heparin-binding EGF-like growth factor stimulates chemotaxis but not proliferation, EMBO J. 16 (1997) 1268–1278.
[4] R. Iwamoto, S. Yamazaki, M. Asakura, S. Takashima, H. Hasuwa, K. Miyado, S. Adachi, M. Kitakaze, K. Hashimoto, G. Raab, D. Nanba, S. Higashiyama, M. Hori, M. Klagsbrun, E. Mekada, Heparin-binding EGF-like growth factor and ErbB signaling is essential for heart function, Proc. Natl. Acad. Sci. USA 100 (2003) 3221–3226.
[5] E. Nishi, A. Prat, V. Hospital, K. Elenius, M. Klagsbrun, *N*-Arginine dibasic convertase is a specific receptor for heparin-binding EGF-like growth factor that mediates cell migration, EMBO J. 20 (2001) 3342–3350.
[6] J. Massague, A. Pandiella, Membrane-anchored growth factors, Annu. Rev. Biochem. 62 (1993) 515–541.
[7] J.G. Naglich, J.E. Metherall, D.W. Russell, L. Eidels, Expression cloning of a diphtheria toxin receptor: identify with a heparin-binding EGF-like growth factor precursor, Cell 69 (1992) 1051–1061.
[8] R. Iwamoto, S. Higashiyama, T. Mitamura, N. Taniguchi, M. Klagsbrun, E. Mekada, Heparin-binding EGF-like growth factor, which acts as the diphtheria toxin receptor, forms a complex with membrane protein DRAP27/CD9, which up-regulates functional receptors and diphtheria toxin activity, EMBO J. 13 (1994) 2322–2330.

[9] T. Mitamura, S. Higashiyama, N. Taniguchi, M. Klagsbrum, E. Mekada, Diphtheria toxin binds to the EGF-like domain of human heparin-binding EGF-like growth factor/diphtheria toxin receptor and inhibits specifically its mitogenic activity, J. Biol. Chem. 270 (1995) 1015–1019.

[10] S. Higashiyama, R. Iwamoto, K. Goishi, G. Raab, N. Taniguchi, M. Klagsbrun, E. Mekada, The transmembrane protein CD9/DRAP27 potentiates the juxtacrine growth factor activity of the membrane-anchored heparin-binding EGF-like growth factor (proHB-EGF), J. Cell Biol. 128 (1995) 929–938.

[11] T. Nakagawa, S. Higashiyama, T. Mitamura, E. Mekada, N. Taniguchi, Amino-terminal processing of cell surface heparin-binding epidermal growth factor-like growth factor up-regulates its juxtacrine but not its paracrine growth activity, J. Biol. Chem. 271 (1996) 30858-30863.

[12] M. Asakura, M. Kitakaze, S. Takashima, Y. Liao, F. Ishikura, T. Yoshinaka, H. Ohmoto, K. Node, K. Yoshino, H. Ishiguro, H. Asanuma, S. Sanada, Y. Matsumura, H. Takeda, S. Beppu, M. Tada, M. Hori, S. Higashiyama, Cardiac hypertrophy is inhibited by antagonism of ADAM12 processing of HB-EGF: metalloproteinase inhibitors as a new therapy, Nat. Med. 8 (2002) 35–40.

[13] D. Nanba, S. Higashiyama, Dual intracellular signaling by proteolytic cleavage of membrane-anchored heparin-binding EGF-like growth factor, Cytokine Growth Factor Rev. 15 (2004) 13–19.

[14] K. Goishi, S. Higashiyama, M. Klagsbrun, N. Nakano, T. Umata, M. Ishikawa, E. Mekada, N. Taniguchi, Phorbol ester induces the rapid processing of cell surface heparin-binding EGF-like growth factor: conversion from juxtacrine to paracrine growth factor activity, Mol. Biol. Cell 6 (1995) 967–980.

[15] D. Nanba, A. Mammoto, K. Hashimoto, S. Higashiyama, Proteolytic release of the carboxy-terminal fragment of proHB-EGF causes nuclear export of PLZF, J. Cell Biol. 163 (2003) 489–502.

[16] J. Bao, D. Wolpowiz, L.W. Role, D.A. Talmage, Back signaling by the Nrg-1 intracellular domain, J. Cell Biol. 161 (2003) 1133–1141.

[17] S.M. Dethlefsen, G. Raab, M.A. Moses, R.M. Adam, M. Klagsburn, M.R. Freeman, Extracellular calcium influx stimulates metalloproteinase cleavage and secretion of heparin-binding EGF-like growth factor independently of protein kinase C, J. Cell. Biochem. 69 (1998) 143–153.

[18] M. Vecchi, L.A. Rudolph-Owen, C.L. Brown, P.J. Dempsey, G. Carpenter, Tyrosine phosphorylation and proteolysis. Pervanadate-induced, metalloprotease-dependent cleavage of the ErbB-4 receptor and amphiregulin, J. Biol. Chem. 273 (1998) 20589–20595.